From Cell to Tissue Properties—Modeling Skin Electroporation With Pore and Local Transport Region Formation

Janja Dermol-Černe and Damijan Miklavčič

***Abstract*—Current models of tissue electroporation either describe tissue with its bulk properties or include cell level properties, but model only a few cells of simple shapes in low-volume fractions or are in two dimensions. We constructed a three-dimensional model of realistically shaped cells in realistic volume fractions. By using a 'unit cell' model, the equivalent dielectric properties of whole tissue could be calculated. We calculated the dielectric properties of electroporated skin. We modeled electroporation of single cells by pore formation on keratinocytes and on the papillary dermis which gave dielectric properties of the electroporated epidermis and papillary dermis. During skin electroporation, local transport regions are formed in the stratum corneum. We modeled local transport regions and increase in their radii or density which affected the dielectric properties of the stratum corneum. The final model of skin electroporation accurately describes measured electric current and voltage drop on the skin during electroporation with long low-voltage pulses. The model also accurately describes voltage drop on the skin during electroporation with short high-voltage pulses. However, our results indicate that during application of short high-voltage pulses additional processes may occur which increase the electric current. Our model connects the processes occurring at the level of cell membranes (pore formation), at the level of a skin layer (formation of local transport region in the stratum corneum) with the tissue (skin layers) and even level of organs (skin). Using a similar approach, electroporation of any tissue can be modeled, if the morphology of the tissue is known.**

***Index Terms*—Franz diffusion cell, local transport region, multiscale approach, numerical modeling, pore formation, skin electroporation.**

I. Introduction

ELECTROPORATION is a physical way of disturbing cell membrane with the application of short, high-voltage pulses leading to increase in its permeability to different molecules (reversible electroporation) and to achieve cell death (IRE - irreversible electroporation) [1], [2]. Electroporation or pulsed electric field treatment is used in biotechnology [3], food-processing [4], [5] and medicine [6], e.g., gene electrotransfer [7], [8], DNA vaccination [9], [10], transdermal drug delivery [11], [12], IRE as an ablation technique [13], [14] and electrochemotherapy [15], [16].

Transdermal drug delivery is easy to conduct, non-invasive, quick and it avoids gastro-intestinal degradation. Skin is also a barrier not many drugs can penetrate, and various enhancement methods are used to improve drug delivery, electroporation being one of them [12]. However, skin electroporation is a complex phenomenon and still not well understood. It is believed that electric pulses cause the formation of regions of an increased electrical conductivity through which the transport occurs – i.e., local transport regions (LTRs). The density of the LTRs increases with increasing voltage while their size increases with increasing pulse duration [17]–[22].

Models of tissue electroporation enhance our understanding as they offer a concise description using mathematical and physical laws. The current tissue models are of two types – they model tissue as a bulk [23]–[26] while only few model tissues' microscopic structure [27]–[31]. The bulk tissue models describe the electric field distribution as a function of tissue properties, applied voltage and the geometry of the electrodes but assume that the tissue is homogeneous. For each tissue type, the critical electric field for electroporation or cell death must be experimentally determined or described with statistical models [32]–[34]. The models with included microstructure are in 2D or 3D. The 2D models include sampling the tissue with Cartesian transport lattices [30], [31], [35], describing it with the equivalent circuit [36], [37], or modeling it with the Voronoi network [29]. The 2D models disregard the geometry of the cells and cannot model different cell density which significantly alters the equivalent dielectric properties, the induced transmembrane voltage and electroporation [38]. In 3D, tissue was modeled as an infinite lattice [39], [40] or randomly distributed spherical cells of different sizes [28]. The volume fraction maximally achievable by face-centered cube or hexagonal close-packed lattices is 77% which is lower than the volume fractions we encounter in most tissues (e.g., 83% in the epidermis, 91% in the stratum corneum, 85% in the muscle tissue, 80% in the hypodermis [41]). Furthermore, cells were not of realistic shapes although it was shown that cell shapes also affects the dielectric properties [42]. An improvement was a model of spinach leaf which also

Manuscript received October 20, 2017; accepted November 8, 2017. Date of publication November 16, 2017; date of current version January 18, 2018. This work was supported by the Slovenian Research Agency (research core funding nos. P2-0249 and IP-0510 and Junior Researcher funding to JDČ). *(Corresponding author: Damijan Miklavčič.)*

J. Dermol-Černe and D. Miklavčič are with the Faculty of Electrical Engineering, University of Ljubljana, Ljubljana SI-1000, Slovenia (e-mail: damijan.miklavcic@fe.uni-lj.si).

Digital Object Identifier 10.1109/TBME.2017.2773126

included the size and shape of the cells; however, only a small part was modeled [27], and a generalization to the whole leaf is questionable. The model by Huclova *et al*. [42] also models single cells but offers a more realistic description since cells can be of different shapes, sizes, and densities. Moreover, also tissue heterogeneity and anisotropy can be described which most of the current models cannot. The dielectric properties of cells are generalized to tissues as their equivalent dielectric properties. Numerical calculation is reduced to tissue level, and much larger geometry than a single cell can be modeled. The latter model describes the behaviour of cells in the linear range but has a potential to include also nonlinear behaviour, i.e., electroporation.

In the field of skin electroporation, only a few models exist [20], [43]–[48] and they mostly belong to the group of bulk tissue models and for the values of dielectric properties of separate layers take rough approximations or even model several layers with the same values. The values of the dielectric properties of the electroporated layers are also rough approximations [44]. Some models include the formation of the local transport regions [43], [46], [48] but are focused only on the stratum corneum and do not include pore formation in the membranes of the cells in lower layers. In the equivalent circuit of the skin [47], the information on the geometry of the cells is lost, and the resistance of the elements is determined by experimental measurements which vary between systems.

Our aim was thus to start from the microscopic scale to obtain a bulk model of skin electroporation. We started with the model by Huclova *et al*. [41] which has several advantages (possibility to model real shapes and densities of cells, heterogeneity and anisotropy). We modeled the change in dielectric parameters of skin during electroporation and validated our model with current-voltage measurements. We modeled pore formation in cell membranes and local transport region formation in the stratum corneum. We modeled the skin's dielectric properties after two protocols which varied in voltage and pulse duration – long low-voltage pulses (LV protocol) and short high-voltage pulses (HV protocol) [49]. We achieved good agreement with measurements of LV protocol by including LTR formation in the stratum corneum, change in electrical conductivity of the deeper skin layers due to cell membrane electroporation and electrode polarisation. During HV protocol the modeled voltage drop on the skin matched the measurements well; however, the current deviated for 50%. Also, the modeled density of the LTRs in the HV protocol was much higher than the experimentally determined values, which indicates that during the HV protocol additional processes may occur which are not yet identified and were thus not included in our model. The advantage of our approach is that it is not limited only to skin electroporation, but electroporation of any tissue can be modeled provided the geometric and dielectric properties of cells constituting the tissue are known.

II. Methods

A. Experimental Work

For fitting and validation of our model, we used experimental results from [49]. In short, 350 μm thick dermatomed porcine ear skin was put between the donor and receiver chamber of the Franz diffusion cell. Porcine ear skin is similar to the human skin regarding layers' thickness, number of hairs, their size and extension depth [50]. Two Pt electrodes were positioned 0.2 cm above and 0.5 cm below the skin. Long low-voltage (3×45 V pulses of 250 ms duration, 100 ms pause – LV protocol) or short high-voltage pulses (3×500 V pulses of 500 μs duration, 500 μs pause – HV protocol) were delivered to the skin. The delivered voltage, the voltage on the skin and current were measured.

According to the model [41], the dermatomed skin consists of four layers: the stratum corneum, the epidermis, the papillary dermis, and the upper vessel plexus.

B. Construction of the Model

The model of the skin before electroporation was constructed according to [41]. The modeling in our study aimed to add electroporation to the model by Huclova *et al*. The main steps in our 'upgraded' model are described by Fig. 1. We manually changed (i.e., optimized) the parameters in the local transport region model and the electroporation in a unit cell model. We obtained equivalent dielectric properties of separate layers and introduced them into the Franz diffusion cell model. We applied voltage to the Franz diffusion cell model and calculated the electric current and the voltage drop on the skin. We compared the simulated values with the measured ones and changed the parameters in the local transport region model and electroporation in a unit cell model until the measured and simulated values matched. Values of dielectric and geometric parameters, used in the final model, are referred to as 'optimized values' although they could be only a local optimal values and not global.

The numerical calculations were done in Comsol Multiphysics (v5.3, Stockholm, Sweden) in 3D unless noted otherwise. All models were remeshed until there was a negligible difference in the modeled voltage drop on the skin with further remeshing. In all models, electric currents physics was used which calculates the electric potential in a subdomain by

$$-\nabla\left(\sigma\nabla \mathrm{V}\right) - \nabla \mathrm{j}\omega\varepsilon\nabla \mathrm{V} = 0 \tag{1}$$

where σ denotes the electric conductivity, ε the relative permittivity of the subdomain. jω in the frequency domain is equivalent to time differentiation in the time domain. Cell membrane was modeled by boundary condition distributed impedance, given by

$$n \cdot J = \frac{1}{d_m}\left(\sigma_m + j\omega\varepsilon\right)\left(V - V_{\mathrm{ref}}\right) \tag{2}$$

where d_m denotes the membrane thickness, ε its dielectric permittivity, σ_m its electrical conductivity, V_{ref} is the electric potential on the exterior side of the boundary, n is the unit vector normal to the boundary surface, J is the electric current density.

1) The Model of Dielectric Properties Without Electroporation: We constructed the model as described in [41]. For more detail on initial geometric and dielectric properties of the cells and settings of the numerical solver, we refer the reader to [41]. The authors modeled full thickness skin and also included layers which were not included in the dermatomed skin from our experiments. Initially, we modeled all layers for validation of our model, but for modeling electroporation, only the stratum

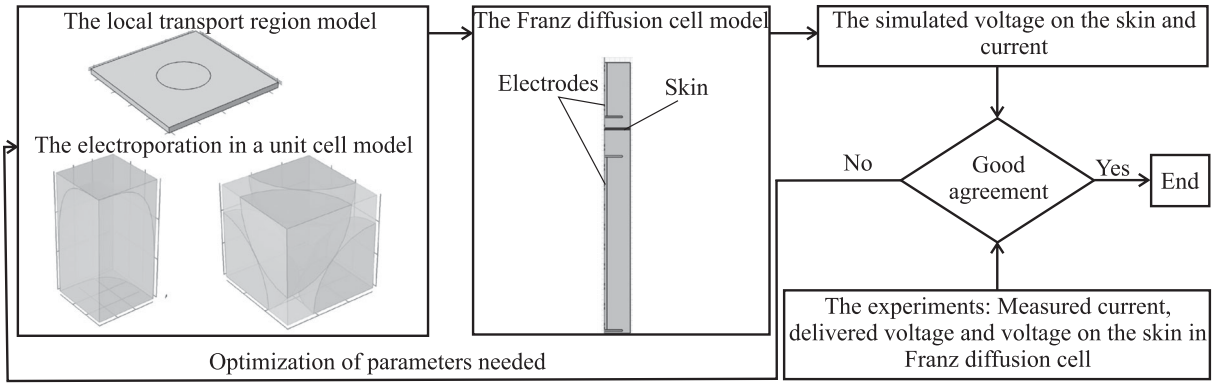

Fig. 1. Optimization scheme used in obtaining the parameters of the skin electroporation model. The parameters of the local transport region model and the electroporation in a unit cell model were changed and introduced into the Franz diffusion cell model. In the Franz diffusion cell model, we simulated the current through the Franz diffusion cell and voltage drop on the skin. Results of the simulation were compared to the results of the experiments. We varied the parameters of the models until the simulated and measured values matched.

corneum, epidermis, papillary dermis, and upper vessel plexus were modeled. Briefly, the skin was divided into separate layers, based on their morphology. In each layer, a typical biological cell (i.e., corneocyte, keratinocyte,) or a typical structure (i.e., blood vessels, collagen fibres) were identified. For the calculation of equivalent dielectric properties, either analytical or numerical method was applied. When the particles were embedded in the extracellular fluid in a low volume fraction (<80%) the analytical Hanai-Bruggeman equation was used in Matlab R2015b (Mathworks, USA) which was calculated much faster than the numerical method. The papillary dermis was modeled as 40 μm spheres in 0.74 volume fraction and the upper vessel plexus as x-axis oriented cylinders with diameter 50 μm in volume fraction 0.3. Layers of higher volume fractions were modeled numerically. A unit cell was constructed for each cell layer. A biological cell in a unit cell was modeled via the 'superformula', imported into the Comsol and scaled to achieve the correct sizes and volume fractions. These were (in x-, y- and z-direction with corresponding volume fraction) for the corneocyte: (40 μm, 40 μm, 0.8 μm, 0.85) and the keratinocyte: (5.97 μm, 5.97 μm, 11.95 μm, 0.8). Several unit cells together could describe the morphology of the entire layer. Stratum corneum was modeled with corneocyte, epidermis with keratinocyte and subcutaneous tissue with adipocyte. In Fig. 2, the corneocyte, the keratinocyte and the papillary dermis (used with the Krassowska asymptotic equation) are shown. The opposite boundaries of the unit cell were exposed to a sinusoidal voltage, and via the admittance, the frequency dependent dielectric properties were calculated (ε^*). Other outer boundaries were set to insulation. The process was repeated in all three axes to obtain the dielectric tensor ($\bar{\bar{\varepsilon}}^*$). From $\bar{\bar{\varepsilon}}^*$, the electrical conductivity and relative permittivity were calculated and inserted in the Franz diffusion cell model as properties of separate layers. We used the frequency domain study, the direct PARDISO solver and the physics controlled mesh with finer or extra fine element size.

2) The Model of Dielectric Properties With Electroporation: We added skin electroporation to the model by Huclova *et al.* [41]. We modeled pore formation on the level of single cells as well as local transport region formation in stratum

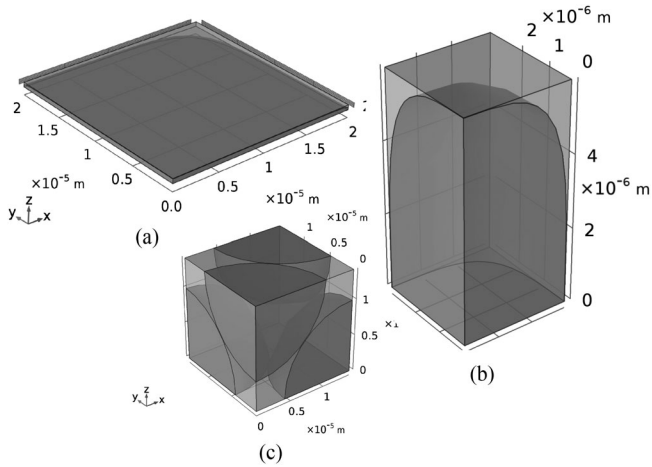

Fig. 2. The geometry of the (a) corneocyte, (b) keratinocyte. Due to the symmetry, only one-eighth was modeled. (c) Spheres in papillary dermis were arranged in the face-centered cubic arrangement and could not be described by including only one cell in the unit cell. Thus, for unit cell, we used a geometry which could periodically describe the geometry of the papillary dermis.

corneum. The pore formation was modeled on the keratinocytes and papillary dermis. The local transport region formation was modeled in the stratum corneum. The upper vessel plexus was assumed not be electroporated.

a) The Model of Pore Formation: Pore formation was included with Krassowska's asymptotic equation [51], [52]. We modeled pore formation on the keratinocytes [Fig. 2(b)] and spheres in the papillary dermis, [Fig. 2(c)]. The Krassowska's asymptotic equation cannot be analytically modeled, and thus we used the papillary dermis unit cell [Fig. 2(c)] and not the Hanai-Bruggeman equation. Papillary dermis was modeled as spheres in the face-centered cubic arrangement in volume fraction 0.74. To include Krassowska's asymptotic equation, we used the Weak Form Boundary Partial Differential Equation interface with

$$\frac{dN}{dt} = \alpha e^{\left(\frac{ITV}{Vep}\right)^2}\left(1 - \frac{N}{N_0}e^{-q\left(\frac{ITV}{Vep}\right)^2}\right), \qquad (3)$$

TABLE I
PARAMETERS USED IN UNIT CELL MODEL WITH KRASSOWSKA'S ASYMPTOTIC EQUATION, THEIR MEANING, VALUE, AND REFERENCE

Symbol	Meaning	Value	Reference
ε_e	Dielectric permittivity of extracellular space (-)	80	[41]
σ_e	Electrical conductivity of extracellular space (S/m)	0.53	[41]
ε_m	Dielectric permittivity of cell membrane (-)	9.4	[41]
σ_{m0}	Initial electrical conductivity of cell membrane (S/m)	10^{-6}	[41]
ε_i	Dielectric permittivity of the intracellular space (-)	50	[41]
σ_i	Electrical conductivity of intracellular space (S/m)	0.12	[41]
d_m	Thickness of the cell membrane (nm)	7	[41]
V_{ep}	Electroporation threshold (mV)	258	[52]
α	Electroporation parameter ($m^{-2}s^{-1}$)	10^9	[52]
q	Electroporation constant	2.46	[52]
N_0	Equilibrium pore density (m^{-2})	1.5×10^9	[52]
R_p	Pore radius (nm)	0.75	[52]
V_{rest}	Resting membrane voltage (mV)	-50	[52]
σ_p	Pore electrical conductivity (S/m)	$\frac{\sigma_e - \sigma_i}{\ln(\frac{\sigma_e}{\sigma_i})}$	[52]
σ_m	Electrical conductivity of the electroporated cell membrane (S/m)	$\sigma_{m0} + \sigma_{ep}$	[52]

where N denotes the density of the pores in the membrane, and N_0 in the unelectroporated membrane, *ITV* the induced transmembrane voltage, α, q, V_{ep} describe the characteristics of the electroporation process [51], [52], and t is time. The pore formation caused an increase in electrical conductivity of the cell membrane:

$$\sigma_{ep} = N \frac{2\pi r_p^2 \sigma_p d_m}{\pi r_p + 2d_m}, \tag{4}$$

where r_p and σ_p were the radius and the internal electrical conductivity of a single pore, respectively, and d_m is the cell membrane thickness. The values of the parameters are in Table I. Increasing voltages were applied to the opposite boundaries of the unit cell in the z-direction. With increasing voltages, the density of the pores increased and consequently the induced transmembrane voltage. Dielectric tensor was calculated via the applied voltage and the current flowing through the unit cell. In the experiments, the pulses were applied in the z-direction, and pore formation was therefore primarily in the z-direction. Electrical conductivity in x- and y-directions and the relative permittivity in all three directions (x, y, z) were assumed unchanged and set to the unelectroporated values. We used the time domain study, the direct PARDISO solver and the physics controlled mesh with finer or extra fine element size.

b) The Model of the Local Transport Region Formation: The effect of electric pulses on the stratum corneum was modeled via local transport region (LTR) formation. The LTR was modeled as a cylinder in a unit cell (Fig. 3). We chose the size of the LTR as stated it [49] and adapted the density by changing the width and depth of the unit cell. In LV protocol, the LTR's diameter was chosen according to [49] and in HV protocol its density was adapted. Also here, we applied voltage on opposite boundaries in x- or z-direction, and via the electric current calculated the dielectric tensor. Due to the symmetry, the properties in the x- and y-axis were the same. The geometric and dielectric properties of the stratum corneum and the LTR are in Table II. The dielectric properties of the electroporated stratum corneum were calculated under DC conditions since the applied pulses in LV and HV protocol were relatively long and the capacitive properties could be neglected. The size of the local transport region was taken from [49] and slightly adapted as we took into account that between pulses the LTRs could partially reseal which allowed a better description of our experimental data. We used frequency domain study, the direct PARDISO solver and the physics-controlled mesh with extra fine element size.

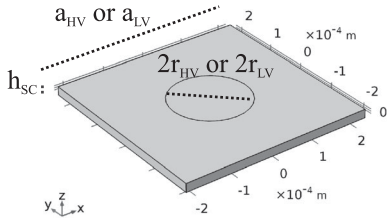

Fig. 3. Geometry of the local transport region (LTR) embedded in the stratum corneum (SC). The cylinder is the LTR. The outer region is the SC, unaffected by electric pulses. The image represents the size and density of the LTR at the end of low-voltage protocol at t = 1 s (a_{LV} was 443 μm and r_{LV} was 90 μm).

TABLE II
GEOMETRIC AND DIELECTRIC PROPERTIES OF THE LOCAL TRANSPORT REGION AND THE UNELECTROPORATED STRATUM CORNEUM, THEIR MEANING, VALUE AND REFERENCE

Symbol	Meaning	Value	Reference/method
ε_{LTR} (x, y, z)	Dielectric permittivity of the LTR (-)	x and y: 6.97×10^4, z: 5.46×10^2	Calculated with a unit cell with unelectroporated corneocyte
σ_{LTR} (isotropic)	Electrical conductivity of the LTR (S/m)	0.7	Optimized*
ε_{SC} (x, y, z)	Dielectric permittivity of the SC (-)	x and y: 6.97×10^4, z: 5.46×10^2	Calculated with a unit cell with unelectroporated corneocyte
σ_{SC} (x, y, z)	Electrical conductivity of the SC (S/m)	x and y: 1.38×10^{-2}, z: 2.29×10^{-4}	Calculated with a unit cell with unelectroporated corneocyte
r_{LV}	Radius of the LTR during LV protocol	Fig. 5(a)	[49]
r_{HV}	Radius of the LTR during HV protocol (μm)	10	[49]
a_{LV}	Length of the unit cell during LV protocol (μm)	443	[49]
a_{HV}	Length of the unit cell during LV protocol (μm)	177, 130, 100, 80, 60, 40, 30 (density in Fig. 6(a))	Optimized*
h_{LTR}	Height of the LTR (μm)	20	The same as the SC height
h_{SC}	Height of the SC (μm)	20	[41], [49], [50]

SC denotes stratum corneum and LTR local transport region.
*Optimization was done by comparing measured and simulated current and voltage drop on the skin.

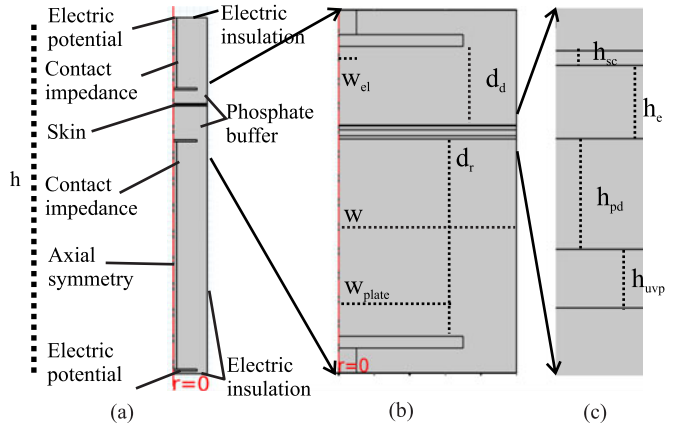

Fig. 4. Geometry of the Franz diffusion cell with marked boundary conditions and geometry. (a) the whole model, (b) zoomed to the area between the electrodes and (c) zoomed to the skin.

c) The Model of Franz Diffusion Cell: The Franz diffusion cell model was built according to the measurements and the data in [49]. In Comsol, we used 2D axisymmetric geometry. Although the properties of the skin were anisotropic, there was only 3% difference in the 2D and 3D calculation. However, the 3D calculation took approximately 6 hours and the 2D 1 minute. The boundary conditions and the geometric parameters of the Franz diffusion cell model are marked in Fig. 4. Between the electrodes, there was skin, immersed in phosphate buffer. On top of the electrodes, we applied the measured square voltage pulses. The other boundaries of the electrodes were assigned contact impedance to model the impedance of the double layer, formed at the electrode-liquid interface:

$$n \cdot J_1 = \frac{1}{\rho}(V_1 - V_2) \tag{5a}$$

$$n \cdot J_1 = \frac{1}{\rho}(V_1 - V_2) \tag{5b}$$

where ρ denotes the surface resistance and V_1 and V_2 are the voltages on each side of the boundary, n is the unit vector normal to the boundary surface, J is the electric current density. Properties of the stratum corneum were obtained from the model of the local transport region, properties of the epidermis from the unit cell of the keratinocyte and applied Krassowska's equation, properties of the papillary dermis from the unit cell of the spheres in the papillary dermis and applied Krassowska's asymptotic equation. We used the physics-controlled mesh with normal element size, time domain study and a direct MUMPS solver.

III. Results

After choosing the size [49] [LV protocol – Fig. 5(a)] and adapting the density [HV protocol – Fig. 6(a)] of the local transport regions (LTRs) we obtained the corresponding equivalent electrical conductivity [Fig. 5(b) LV protocol and Fig. 6(b) HV protocol] and relative permittivity [Fig. 5(c) LV protocol and Fig. 6(c) HV protocol]. Fig. 5 thus shows results for the LV protocol – in Fig. 5(a) we can see how the radius of the LTR changed during the treatment, in Fig. 5(b) the change in the equivalent electrical conductivity and Fig. 5(c) in equivalent relative permittivity in all three directions (x, y, and z). Fig. 6 shows results for the HV protocol – on Fig. 6(a) we can see how the density of LTRs changed during the treatment, in Fig. 6(b) the change in the equivalent electrical conductivity and Fig. 6(c) in equivalent relative permittivity in all three directions (x, y, and z).

Fig. 7 shows the electrical conductivity of lower layers (papillary dermis and epidermis) as calculated using the Krassowska's asymptotic equation. The electrical conductivity varies with different voltages on the boundary of the unit cell. Optimized values of the electrical conductivity were inserted in the Franz, diffusion model. Figs. 8 and 9 show the final results of our model – the simulated values of the voltage on the skin and the current and are compared with the measured values. In the LV protocol (Fig. 8) the simulated and measured values of the voltage drop on the skin [Fig. 8(a)] and the current [Fig. 8(b)] matched well while in the HV protocol [Fig. 9] the voltage drop on the skin corresponded well [Fig. 9(a)], but the current did not [Fig. 9(b)]. The simulated current underestimated the actual measurement for approximately 50%.

IV. Discussion

A. Experimental Considerations

In the stratum corneum (SC), the local transport regions (LTRs) were formed. In the epidermis (E) and papillary dermis (PD), cell electroporation occurred as SC resistance decreased due to LTR formation, and consequently, electric field increased also in the lower layers. Electric pulses increase the permeability of blood vessels and induce vascular lock [55], [56]. However, we assumed there was no electroporation in the upper vessel plexus (UVP) as it is a layer of blood vessels and even if we assumed electroporation to occur there is a lack of experimental data on its dielectric properties after electroporation.

Change in dielectric properties of tissues can be used to describe and understand processes happening during electroporation. For assessing skin permeability, electric measurements were used before [17], [57]–[60]. Dielectric properties can be measured by dielectric spectroscopy [61], current-voltage measurements during electroporation [62], electric impedance tomography [63], and magnetic resonance electric impedance tomography [64]. The efficiency of electroporation can be monitored by measurements of the change in electrical conductivity [25], [65], [66]. When measuring dielectric properties of tissues, secondary effects can affect measurements – such as swelling of cells [67], forming of edema [65], loss of ions from the cells [62], vascular lock [55]. Thus, for the validation of our model, we used current-voltage measurements during pulse application when the secondary effects can still be largely neglected.

Skin hydration and the electrical conductivity of the liquid in which the skin is immersed was shown to have a large effect on skin impedance [68]. In our experiments, the dermatomed skin was well hydrated as it was immersed in phosphate buffer. We took hydration into account by increasing the electrical conductivity of LTRs to 0.7 S/m. This conductivity is in the same range as in [43] but is much higher than the electrical conductivity of

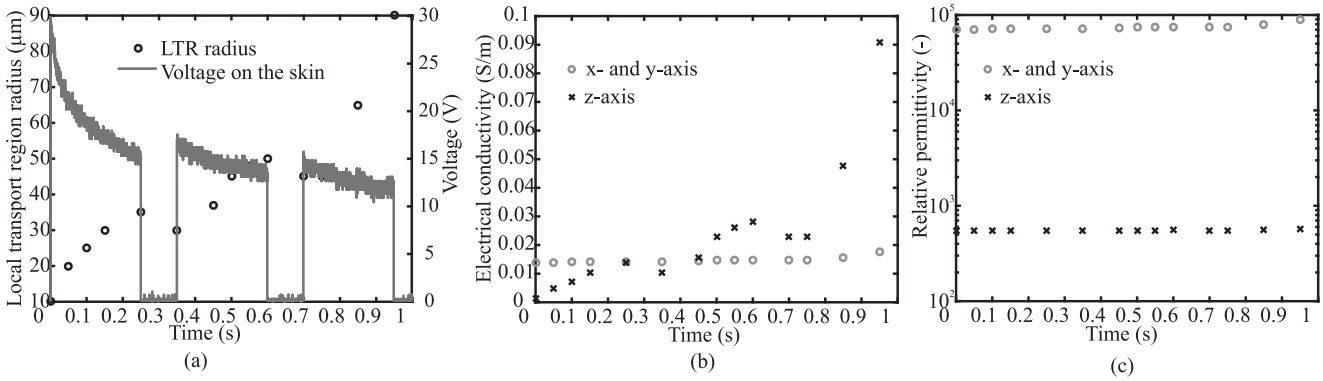

Fig. 5. Dynamics of local transport region (LTR) during low-voltage (LV) protocol. (a) LTR size and the corresponding voltage on the skin, (b) electrical conductivity and (c) relative permittivity change. The obtained values were then taken as equivalent dielectric properties of the whole stratum corneum. The axes correspond to the coordinate system in Fig. 3.

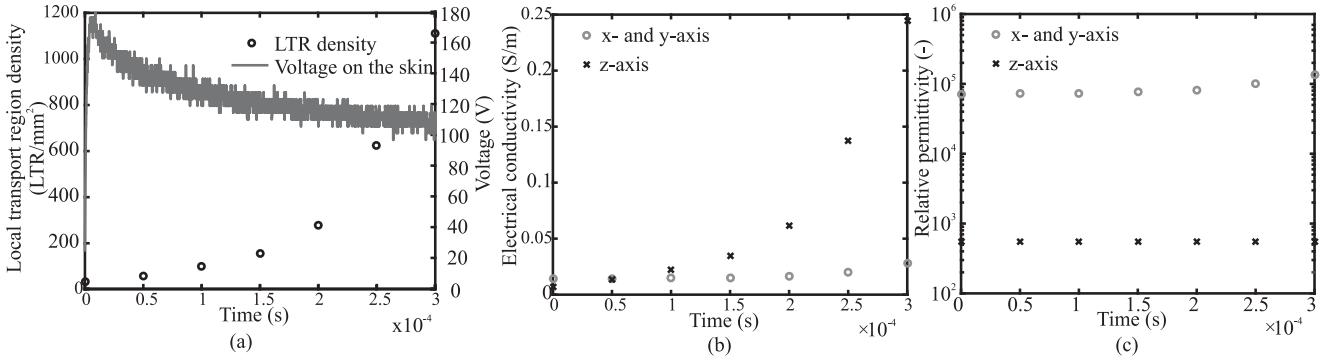

Fig. 6. Dynamics of local transport region (LTR) during high-voltage (HV) protocol. (a) LTR density and the corresponding voltage on the skin, (b) electrical conductivity and (c) relative permittivity change. The obtained values were then taken as equivalent dielectric properties of the whole stratum corneum. Please, notice the time-scale which is only 300 μs although the whole treatment took 2.5 ms. We assumed that all changes in the LTR density occur during the first pulse and afterwards there was no resealing or increasing of the LTR density. The axes correspond to the coordinate system in Fig. 3.

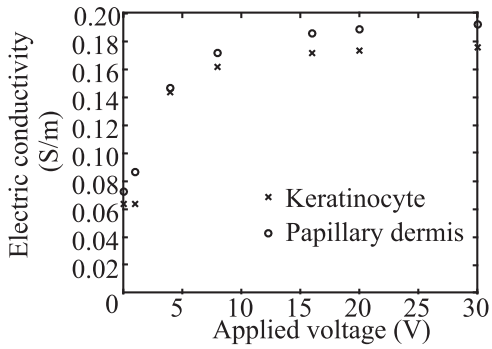

Fig. 7. Electrical conductivity as a function of voltage, applied to a unit cell of a keratinocyte or papillary dermis. Even before pulse formation, the unit cell has a certain conductivity which then increases as a function of applied voltage.

melted lipids (0.05 S/m [49]) which is relevant in the case of dry skin.

We assumed that the relative permittivity of the epidermis, papillary dermis and upper vessel plexus do not change due to electroporation since the applied pulses were long and the capacitive component of the layers at low frequencies is approximated with an open circuit. The change in relative permittivity of the stratum corneum was based on the change in the geometry of the LTR.

The buffer used in the donor compartment was phosphate buffer, and in the receiver, it was phosphate buffered saline. They varied in the ionic composition and pH, but their electrical conductivity was the same (1 S/m). For our model, only the dielectric properties were important, and we modeled liquid in the donor and receiver compartment as the same buffer.

B. Pore Formation in Keratinocytes and Papillary Dermis

The Krassowska's asymptotic equation describes how the density of the pores changes as a function of applied voltage and time. It is a simplification of a theory of pore formation as it assumes all pores in the cell membrane are of the same size which is a justified approximation only for short nanosecond pulses. During longer pulses, the pores start to grow. For inclusion of an increase in pore radius, creation of stable macropores should be modeled [69], but the inclusion is computationally demanding. Therefore, we decided to calculate the change of electrical conductivity in the first few nanoseconds by Krassowska's asymptotic equation. As the sampling period of the current and voltage

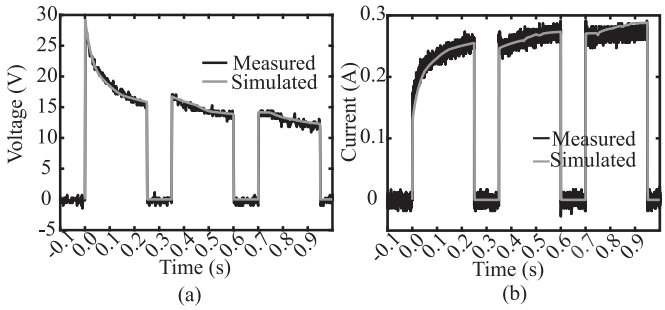

Fig. 8. Measured and simulated (a) voltage on the skin and (b) current through the system during LV protocol.

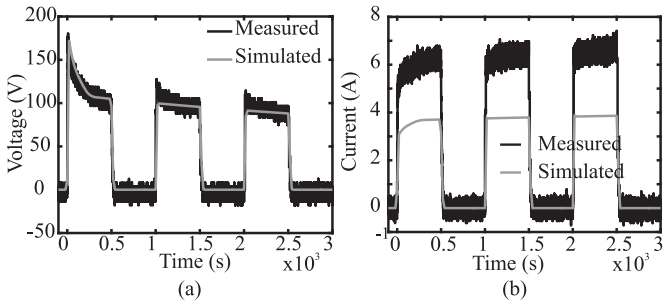

Fig. 9. Measured and simulated (a) voltage on the skin and (b) current through the system during HV protocol.

measurements was much longer than nanoseconds, we assumed that the electrical conductivity of the papillary dermis and the epidermis changed immediately when the pulse was applied. We calculated the dielectric properties at $t = 0\,\mathrm{s}$ by the Krassowska's asymptotic equation. To avoid modeling pore growth, we simplified our model and adapted the bulk electrical conductivity of separate layers at the end of pulse application. The dielectric properties during pulse application were determined by interpolation between $t = 0\,\mathrm{s}$ and $t = 1\,\mathrm{s}$ (LV protocol) or $t = 2.5\,\mathrm{ms}$ (HV protocol). The changes in electrical conductivity of lower layers (papillary dermis and epidermis) had to be included; otherwise we could not describe the experimental measurements.

The initial electrical conductivity of the epidermis and papillary dermis was for the LV protocol approximated with Krassowska's equation when 0.07 V or 0.08 V were applied to the unit cell which corresponds to 69 mV or 71 mV of induced transmembrane voltage for corneocyte and papillary dermis, respectively. The initial electrical conductivity of the epidermis and papillary dermis was for the HV protocol approximated with Krassowska's equation when 3 V were applied to the unit cell which corresponds to 1.14 V or 1.24 V of induced membrane voltage for corneocyte and papillary dermis, respectively. The initial theoretical voltage drop at $\mathrm{t} = 0\,\mathrm{s}$ on the epidermis and papillary dermis was determined by treating skin as a voltage divider (right part of Fig. 10) on which there was a 30 V [LV protocol – initial peak of Fig. 8(a)] or 180 V [HV protocol – initial peak on Fig. 9(a)] voltage drop. Taking into account the geometry (thickness of layers, area $0.785\,\mathrm{cm}^2$ [49], size of unit cells and corresponding number of unit cells in z-direction) and

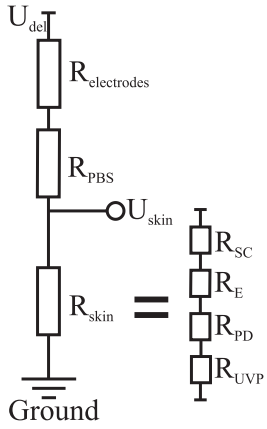

Fig. 10. The equivalent circuit of the Franz diffusion cell. The electrode polarisation is represented only by resistance. Since we are delivering relatively long pulses, the capacitance due to a double layer which is in parallel with $R_{\mathrm{electrodes}}$, could be approximated as an open circuit and thus neglected. $\mathrm{R_{skin}}$ is represented by separate resistances of each layer. The voltage drop on the skin is thus distributed among $\mathrm{R_{SC}}$, $\mathrm{R_E}$, $\mathrm{R_{PD}}$ and $\mathrm{R_{UVP}}$, according to the thickness and electric conductivity of each layer.

initial electrical conductivity of each layer before electroporation in z-direction (SC: 2.29×10^{-4} S/m, E: 6.36×10^{-2} S/m, PD: 7.19×10^{-2} S/m, UVP: 3.85×10^{-1} S/m) we calculated the resistance of each layer and a corresponding voltage drop on each layer. This calculated voltage drop was then used in the Krassowska's asymptotic model.

With HV protocol, the initial theoretical voltage drop on the epidermis and papillary dermis was 0.4 V, but a good agreement between measurements and model was achieved with 3 V. The initial electrical conductivity was thus higher than theoretically predicted. Higher initial electrical conductivity indicates that some defects were formed in the stratum corneum quickly and lower layers were exposed to a higher voltage than predicted.

In HV pulses, the change in electrical conductivity was the largest during the first pulse, and it changed only slightly during the following two pulses. Between pulses, there was some decrease in electrical conductivity present which indicates resealing of the cell membranes as defects in the stratum corneum were reported to reseal on a timescale of ms - hours [22].

C. Local Transport Region Formation in the Stratum Corneum

It was shown that short high-voltage pulses increase the density of the local transport regions (LTRs) while low-voltage long pulses increase the size of LTRs by Joule heating and lipid melting around the pre-existing defects [17]–[22]. The radius of the LTR during LV protocol increased from 10 μm to 90 μm and was taken from [49] and the values are within the ranges reported by [21], [22]. We assumed that LTRs reseal to some extent between pulses [Fig. 6(a)] although as with the HV protocol, it is possible that cells in the lower layers resealed as well. Since the pause during LV protocol was longer than during HV protocol (100 ms vs 500 μs), we modeled LTR resealing instead of corneocyte or papillary dermis resealing. The time course of recovery in skin electroporation ranges from a few ms up to

several hours [22]. Thus, we assumed that it is possible that LTR radii slightly decrease during the pause between pulses. Still, this is only an assumption – the increase in the resistance of the skin could as well be a consequence of resealing of the pores in the membranes of the cells in the lower layers. We have added the resealing in our model, and by doing so, we were able to describe the measurements of voltage and current more accurately.

The increase in electrical conductivity of SC during HV protocol was modeled by an increase in density of the LTRs while their radii stayed the same (10 μm). The modeled density of the LTR-s was high (up to 1200 LTRs/mm^2) in comparison to previously published studies ([43] and the references therein) (up to 9 LTR/mm^2). We tried decreasing the density of the LTRs down to the reported values, but the modeled voltage on the skin was 2-times higher than measured which indicates that with lower LTR density the predicted electrical conductivity of the skin is too low. Even with increasing the electrical conductivity of epidermis and papillary dermis to 1 S/m (electrical conductivity of the phosphate buffer), the voltage on the skin did not decrease enough to obtain voltage on the skin that would correspond to the measured values. This indicates that LTR density is most probably higher than expected.

D. Measurements and Simulation in the Franz Diffusion Cell

An equivalent circuit can represent the Franz diffusion cell (Fig. 10), where $R_{\mathrm{electrodes}}$, R_{PBS} and R_{skin} denote the resistance of the double layer on the electrodes, phosphate buffer and skin, respectively. U_{del} is the voltage, delivered to the electrodes, and U_{skin} the voltage, measured on the skin. The double layer acts as an additional resistance in parallel to capacitance [53]. Since our pulses were relatively long, we assumed the capacitance as an open circuit, and only the resistance $R_{\mathrm{electrodes}}$ was included in the equivalent circuit (Fig. 10). This additional resistance caused a drop of voltage on the electrodes, and the sample received less voltage than what was delivered to electrodes. In the case of LV protocol, the voltage drop on electrodes was significant in comparison to the applied voltage and voltage drop on the skin (around 1 V on the electrodes with delivered 45 V and 12–30 V on the skin). In the case of HV protocol, the voltage drop on the electrodes did not influence the results but was included for consistency. $R_{\mathrm{electrodes}}$, R_{PBS}, U_{del}, and U_{skin} were known, which means that according to the voltage divider, R_{skin} is already determined:

$$R_{\mathrm{skin}} = \frac{U_{\mathrm{skin}}\left(R_{\mathrm{electrodes}} + R_{PBS}\right)}{U_{\mathrm{del}} - U_{\mathrm{skin}}} \tag{6}$$

The simulated voltage drop on the skin and current through the system after the LV protocol corresponded well with the measurements (Fig. 8). The fitting was obtained by adapting the electrical conductivities of separate layers until a good agreement was obtained between simulated and measured values. Taking into account that in LV protocol, the simulated and measured current match [Fig. 8(b)], our model was thus additionally validated.

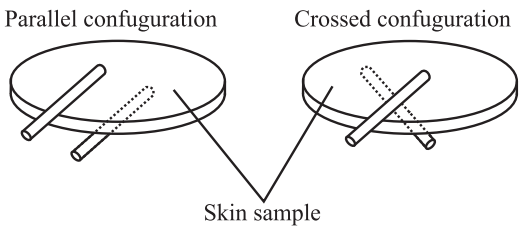

Fig. 11. Position of the measuring Cu electrodes. When in parallel, the electrodes were not directly one on top of another as they would squeeze the skin and change the thickness of the skin. When the electrodes were crossed, there was a preferential path for electric current.

In HV protocol, however, when we achieved a good agreement between simulated and measured voltage drop on the skin, the simulated and measured current did not match [Fig. 9(b)]. One possibility is additional processes, e.g., introduced by measuring Cu electrodes. Namely, when measuring the voltage drop on the skin, the Cu electrodes were in contact with skin. The electrodes were put on the skin between the donor and receiver part of the Franz diffusion chamber in two possible configurations: parallel and crossed (Fig. 11) (M. Reberšek, personal communication). Unfortunately, the exact position of the measuring electrodes was not noted during experiments and is thus not known. Crossed configuration introduced a preferential path for electric current since Cu is much more conductive than PBS or skin. It possible that there was localised heating and discharges present which caused the current to increase significantly, locally thus contributing to the overall current measured, but not causing a detectable voltage drop.

The shape of the voltage and current measurements reflects the different phenomena occurring during electroporation. The initial voltage drop and increase in current in the first few milliseconds is due to LTR formation in the stratum corneum. The emergence of LTRs increases the electric conductivity, but with increasing the radius of the LTRs, the effect slowly reaches a plateau. With decreasing resistance of the SC, the electric field increases in the lower layers of the skin. The prolonged decrease in voltage and increase in current is due to a slow but constant increase in the electric conductivity of lower layers due to pore formation in the cell membranes of the cells in the lower layers, i.e., electroporation.

From Table III we can see that HV protocol increased the electrical conductivity of all layers more than the LV protocol. In LV protocol, the delivered voltage was 45 V, and on the skin, it was 12 V–30 V (26%–66% of the delivered voltage). In HV protocol, the delivered voltage was 500 V, and on the skin, it was 100 V–180 V (20%–36% of the delivered voltage), which is much less than what was delivered to the skin in the LV protocol.

When electrodes are immersed in liquid, a double layer is formed at the electrode-liquid interface. The surface resistance due to the double layer changes with current density, electrode material, ions in the liquid. Interestingly, although it can significantly change the voltage the cells and tissues are exposed to, it is included only in a few models [70]. We used the values

TABLE III
GEOMETRIC AND DIELECTRIC PARAMETERS OF THE FRANZ DIFFUSION CELL MODEL, THEIR MEANING, VALUE AND REFERENCE

Parameter	Meaning	Value	Reference/ Method
w	Radius of the skin sample (cm)	0.5	[49]
h_{sc}	Height of SC (μm)	20	[41], [49], [50]
h_e	Height of E (μm)	100	[41]
h_{pd}	Height of PD (μm)	140	[41]
h_{uvp}	Height of UVP (μm)	80	[41]
d_d	Distance between electrode in the donor solution and skin (cm)	0.2	[49]
d_r	Distance between electrode in the receiver solution and skin (cm)	0.5	[49]
T	Temperature of the FDC (°C)	37	[49]
w_{plate}	Radius of the plate on the electrode (mm)	3.5	[49]
w_{el}	Radius of the electrode (mm)	0.5	[49]
h	Height of the FDC (cm)	5.255	Measured
ρ_s	Surface resistance (Ωcm^2)	3.03	[53]
ε_{PBS}	Dielectric permittivity of the PBS(-)	80	[52]
σ_{PBS}	Electric conductivity of the PBS (S/m)	1	[49]
σ_{el}	Electric conductivity of the Pt electrodes (S/m)	9.43×10^6	[54]
$\varepsilon_{SC,LV}$ (x, y, z)	Dielectric permittivity of the SC after LV protocol (-)	Fig. 5(c)	Optimized*
$\sigma_{SC,LV}$ (x, y, z)	Electric conductivity of the SC after LV protocol (S/m)	Fig. 5(b)	Optimized*
$\varepsilon_{SC,HV}$ (x, y, z)	Dielectric permittivity of the SC after HV protocol (-)	Fig. 6(c)	Optimized*
$\sigma_{SC\,HV}$ (x, y, z)	Electrical conductivity of the SC after HV protocol (S/m)	Fig. 6(b)	Optimized*
ε_E (x, y, z)	Dielectric permittivity of the E (-)	x and y: 4.83×10^3, z: 1.52×10^4	The unit-cell model with keratinocyte
$\sigma_{E,LV}$ (x, y, z)	Electrical conductivity of the E after LV protocol (S/m)	x and y: 5.82×10^{-2}, z: 6.36×10^{-2} at $t = 0$ and 7.69×10^{-2} at $t = 1$ s	Optimized*
$\sigma_{E,HV}$ (x, y, z)	Electrical conductivity of the E after HV protocol (S/m)	x and y: 5.82×10^{-2}, z: 0.12 at $t = 0$ and 0.17 at $t = 2.5$ ms	Optimized*
ε_{PD} (isotropic)	Dielectric permittivity of the PD (-)	1.62×10^4	The Hanai-Bruggeman equation
$\sigma_{PD,LV}$ (isotropic)	Electrical conductivity of the PD after LV protocol (S/m)	0.086 at $t = 0$, 0.096 at $t = 1$ s	Optimized*
$\sigma_{PD,HV}$ (isotropic)	Electrical conductivity of the PD after HV protocol (S/m)	0.13 at $t = 0$, 0.18 at t = 2.5 ms	Optimized*
ε_{UVP} (x, y, z)	Dielectric permittivity of the UVP (-)	x: 4.92×10^4, y and z: 6.40×10^4,	The Hanai-Bruggeman equation
σ_{UVP} (x, y, z)	Electrical conductivity of the UVP (S/m)	0.42, 0.39, 0.39	The Hanai-Bruggeman equation

(x, y and z) denote the anisotropic properties in x-, y- and z-direction. SC denotes stratum corneum, E epidermis, PD papillary dermis, UVP upper vessel plexus, PBS phosphate buffer, and FDC the Franz diffusion cell. Dielectric permittivity of material was not relevant as it did not influence the results since the pulses were relatively long.
*Optimization was done by comparing measured and simulated current and voltage drop on the skin.

from a study [53] where they used Pt electrodes. However, they measured resistance in saline instead of phosphate buffer, and their electrodes were smaller, which could affect the results. More concerning is that they delivered much lower voltage than the voltage delivered in our experiments. The chemistry of high voltage pulses delivered to an electrolyte is still not well understood [71], with few studies focusing on the release of metal from electrodes [72] and possible reactions happening on or near the electrodes [73], [74].

The drawback of our model is that there are several combinations of parameters which can offer good agreement with the current and voltage measurements – e.g., we could change the dynamics of local transport region formation and describe the exponential decrease of voltage drop on the skin with different dynamics of change of electrical conductivity of lower layers. We could compensate for the different geometry of the LTRs with a different electric conductivity of the LTR. The model, obtained in this study, is not trying to replicate the experimental results precisely but serves as a proof of principle how cell level electroporation can be expanded to tissue level electroporation. For a more precise determination of parameters, more experiments and electrical measurements are needed as the values of several parameters are currently only estimated (for example, dielectric properties of separate layers during electroporation).

The advantage of using our model is that we can use it to describe any tissue with any resolution we want, we can include blood vessels, lymphatic system, different types of cells in a tissue etc. The only requirement is that the geometric and dielectric properties of the tissues' microstructure are known. When generalizing the properties to a tissue level, the computations are quick and enable inclusion of other physical phenomena – for example, heating or chemical reactions.

V. CONCLUSION

Our model connects the processes occurring at the level of cell membranes (pore formation), and at the level of a skin layer (formation of local transport region in the stratum corneum), with the level of tissue (skin layers) and even level of organs (skin). It enables description and prediction of changes in dielectric properties of tissue while taking into account microstructure and processes on a much smaller scale and simultaneously keeping the computational times reasonable. Not just skin but any other tissue could be described similarly, as long as its microstructure is known. Our model thus offers a step forward in modeling of electroporation at different spatial scales.

ACKNOWLEDGMENT

J. Dermol-Černe would like to thank Dr. Huclova and Dr. Fröhlich for their help with reconstructing the original model, and Dr. Kos and Dr. Rems for their help with Comsol modeling. The research was conducted in the scope of the electroporation in Biology and Medicine (EBAM) European Associated Laboratory (LEA).

References

[1] T. Kotnik *et al.*, "Cell membrane electroporation- Part 1: The phenomenon," *IEEE Elect. Insul. Mag.*, vol. 28, no. 5, pp. 14–23, Sep./Oct. 2012.

[2] T. Y. Tsong, "Electroporation of cell membranes," *Biophys. J.*, vol. 60, no. 2, pp. 297–306, Aug. 1991.

[3] T. Kotnik *et al.*, "Electroporation-based applications in biotechnology," *Trends Biotechnol.*, vol. 33, no. 8, pp. 480–488, Jun. 2015.

[4] S. Mahnič-Kalamiza *et al.*, "Electroporation in food processing and biorefinery," *J. Membrane Biol.*, vol. 247, no. 12, pp. 1279–1304, Dec. 2014.

[5] S. Toepfl *et al.*, "Overview of pulsed electric fields processing for food," in *Emerging Technologies for Food Processing*, Amsterdam, The Netherlands: Elsevier, 2014, pp. 93–114.

[6] M. L. Yarmush *et al.*, "Electroporation-Based technologies for medicine: Principles, applications, and challenges," *Annu. Rev. Biomed. Eng.*, vol. 16, no. 1, pp. 295–320, Jul. 2014.

[7] A. I. Daud *et al.*, "Phase I trial of interleukin-12 plasmid electroporation in patients with metastatic melanoma," *J. Clin. Oncol.*, vol. 26, no. 36, pp. 5896–5903, 2008.

[8] R. Heller and L. C. Heller, "Gene electrotransfer clinical trials," in *Advances in Genetics*, Amsterdam, The Netherlands: Elsevier, 2015, vol. 89, pp. 235–262.

[9] C. L. Trimble *et al.*, "Safety, efficacy, and immunogenicity of VGX-3100, a therapeutic synthetic DNA vaccine targeting human papillomavirus 16 and 18 E6 and E7 proteins for cervical intraepithelial neoplasia 2/3: a randomised, double-blind, placebo-controlled phase 2b trial," *The Lancet*, vol. 386, no. 10008, pp. 2078–2088, Nov. 2015.

[10] S. Vasan *et al.*, "In Vivo electroporation enhances the immunogenicity of an HIV-1 DNA vaccine candidate in healthy volunteers," *PLoS ONE*, vol. 6, no. 5, May 2011, Art. no. e19252.

[11] A. -R. Denet *et al.*, "Skin electroporation for transdermal and topical delivery," *Adv. Drug Del. Rev.*, vol. 56, no. 5, pp. 659–674, Mar. 2004.

[12] B. Zorec *et al.*, "Active enhancement methods for intra- and transdermal drug delivery: A review," *Zdravniski Vestnik*, vol. 82, no. 5, pp. 339–56, 2013.

[13] C. Jiang *et al.*, "A review of basic to clinical studies of irreversible electroporation therapy," *IEEE Trans. Biomed. Eng.*, vol. 62, no. 1, pp. 4–20, Jan. 2015.

[14] H. J. Scheffer *et al.*, "Irreversible electroporation for nonthermal tumor ablation in the clinical setting: A systematic review of safety and efficacy," *J. Vascular Interventional Radiol.*, vol. 25, no. 7, pp. 997–1011, Jul. 2014.

[15] B. Mali *et al.*, "Antitumor effectiveness of electrochemo-therapy: A systematic review and meta-analysis," *Eur. J. Surg. Oncol.*, vol. 39, pp. 4–16, 2013.

[16] D. Miklavčič *et al.*, "Electrochemotherapy: From the drawing board into medical practice," *Biomed. Eng. OnLine*, vol. 13, no. 1, p. 29, 2014.

[17] R. Vanbever *et al.*, "Comparison of the effects of short, high-voltage and long, medium-voltage pulses on skin electrical and transport properties," *J. Controlled Release*, vol. 60, no. 1, pp. 35–47, Jun. 1999.

[18] M. R. Prausnitz *et al.*, "Imaging regions of transport across human stratum corneum during High-Voltage and Low-Voltage exposures," *J. Pharm. Sci.*, vol. 85, no. 12, pp. 1363–1370, Dec. 1996.

[19] U. F. Pliquett *et al.*, "Local transport regions (LTRs) in human stratum corneum due to long and short 'high voltage' pulses," *Bioelectrochem. Bioenergetics*, vol. 47, no. 1, pp. 151–161, Nov. 1998.

[20] J. C. Weaver *et al.*, "Theory of electrical creation of aqueous pathways across skin transport barriers," *Adv. Drug Del. Rev.*, vol. 35, no. 1, pp. 21–39, Jan. 1999.

[21] U. F. Pliquett *et al.*, "Imaging of fluorescent molecule and small ion transport through human stratum corneum during high voltage pulsing: Localized transport regions are involved," *Biophys. Chem.*, vol. 58, no. 1/2, pp. 185–204, Jan. 1996.

[22] T. R. Gowrishankar *et al.*, "Changes in skin structure and electrical properties following high voltage exposure," *Ann. New York Acad. Sci.*, vol. 888, pp. 183–194, Oct. 1999.

[23] D. Šel *et al.*, "Sequential finite element model of tissue electropermeabilization," *IEEE Trans. Biomed. Eng.*, vol. 52, no. 5, pp. 816–827, May 2005.

[24] S. Čorović *et al.*, "In Vivo muscle electroporation threshold determination: realistic numerical models and In Vivo experiments," *J. Membrane Biol.*, vol. 245, no. 9, pp. 509–520, Sep. 2012.

[25] R. E. Neal 2nd *et al.*, "Experimental characterization and numerical modeling of tissue electrical conductivity during pulsed electric fields for irreversible electroporation treatment planning," *IEEE Trans. Biomed. Eng.*, vol. 59, no. 4, pp. 1076–1085, Apr. 2012.

[26] N. Pavšelj and D. Miklavčič, "Numerical modeling in electroporation-based biomedical applications," *Radiol. Oncol.*, vol. 42, no. 3, pp. 159–168, 2008.

[27] K. Dymek *et al.*, "Modeling electroporation of the non-treated and vacuum impregnated heterogeneous tissue of spinach leaves," *Innov. Food Sci. Emerging Technol.*, vol. 29, pp. 55–64, May 2015.

[28] M. Essone Mezeme *et al.*, "A numerical analysis of multicellular environment for modeling tissue electroporation," *Appl. Phys. Lett.*, vol. 100, no. 14, 2012, Art. no. 143701.

[29] R. P. Joshi *et al.*, "Model assessment of cell membrane breakdown in clusters and tissues under High-Intensity electric pulsing," *IEEE Trans. Plasma Sci.*, vol. 36, no. 4, pp. 1680–1688, Aug. 2008.

[30] D. A. Stewart Jr. *et al.*, Cylindrical cell membranes in uniform applied electric fields: Validation of a transport lattice method," *IEEE Trans. Biomed. Eng.*, vol. 52, no. 10, pp. 1643–1653, Oct. 2005.

[31] T. R. Gowrishankar and J. C. Weaver, "An approach to electrical modeling of single and multiple cells," in *Proc. Nat. Acad. Sci.*, Mar. 2003, vol. 100, no. 6, pp. 3203–3208.

[32] J. Dermol and D. Miklavčič, "Predicting electroporation of cells in an inhomogeneous electric field based on mathematical modeling and experimental CHO-cell permeabilization to propidium iodide determination," *Bioelectrochemistry*, vol. 100, pp. 52–61, Dec. 2014.

[33] J. Dermol and D. Miklavčič, "Mathematical models describing chinese hamster ovary cell death due to electroporation in vitro," *J. Membrane Biol.*, vol. 248, no. 5, pp. 865–881, Oct. 2015.

[34] A. Golberg and B. Rubinsky, "A statistical model for multidimensional irreversible electroporation cell death in tissue," *Biomed. Eng. OnLine*, vol. 9, no. 1, p. 13, 2010.

[35] A. T. Esser *et al.*, "Towards solid tumor treatment by nanosecond pulsed electric fields," *Technol. Cancer Res. Treatment*, vol. 8, no. 4, pp. 289–306, Aug. 2009.

[36] A. Ramos, "Effect of the electroporation in the field calculation in biological tissues," *Artif. Organs*, vol. 29, no. 6, pp. 510–513, Jun. 2005.

[37] A. Ramos *et al.*, "A new computational approach for electrical analysis of biological tissues," *Bioelectrochemistry*, vol. 59, no. 1/2, pp. 73–84, Apr. 2003.

[38] R. Susil *et al.*, "Electric field induced transmembrane potential depends on cell density and organization," *Electro- Magnetobiol.*, vol. 17, no. 3, pp. 391–399, 1998.

[39] A. Ramos, "Improved numerical approach for electrical modeling of biological cell clusters," *Med. Biol. Eng. Comput.*, vol. 48, no. 4, pp. 311–319, Apr. 2010.

[40] M. Pavlin *et al.*, "Dependence of induced transmembrane potential on cell density, arrangement, and cell position inside a cell system," *IEEE Trans. Biomed. Eng.*, vol. 49, no. 6, pp. 605–612, Jun. 2002.

[41] S. Huclova *et al.*, "Modelling and validation of dielectric properties of human skin in the MHz region focusing on skin layer morphology and material composition," *J. Phys. Appl. Phys.*, vol. 45, no. 2, Jan. 2012, Art. no. 025301.

[42] S. Huclova *et al.*, "Modelling effective dielectric properties of materials containing diverse types of biological cells," *J. Phys. Appl. Phys.*, vol. 43, no. 36, Sep. 2010, Art. no. 365405.

[43] N. Pavšelj and D. Miklavčič, "Numerical models of skin electropermeabilization taking into account conductivity changes and the presence of local transport regions," *IEEE Trans. Plasma Sci.*, vol. 36, no. 4, pp. 1650–1658, Aug. 2008.

[44] N. Pavšelj *et al.*, "A numerical model of skin electropermeabilization based on In Vivo experiments," *Ann. Biomed. Eng.*, vol. 35, no. 12, pp. 2138–2144, Nov. 2007.

[45] S. Becker *et al.*, "Transdermal transport pathway creation: Electroporation pulse order," *Math. Biosci.*, vol. 257, pp. 60–68, Nov. 2014.

[46] S. M. Becker and A. V. Kuznetsov, "Local temperature rises influence in vivo electroporation pore development: A numerical stratum corneum lipid phase transition model," *J. Biomech. Eng.*, vol. 129, no. 5, pp. 712–721, 2007.

[47] Y. A. Chizmadzhev *et al.*, "Electrical properties of skin at moderate voltages: contribution of appendageal macropores," *Biophys. J.*, vol. 74, no. 2, pp. 843–856, Feb. 1998.

[48] S. Becker, "Transport modeling of skin electroporation and the thermal behavior of the stratum corneum," *Int. J. Thermal Sci.*, vol. 54, pp. 48–61, Apr. 2012.

[49] B. Zorec *et al.*, Skin electroporation for transdermal drug delivery: The influence of the order of different square wave electric pulses," *Int. J. Pharmaceutics*, vol. 457, no. 1, pp. 214–223, Nov. 2013.

[50] U. Jacobi *et al.*, "Porcine ear skin: An in vitro model for human skin," *Skin Res. Technol.*, vol. 13, no. 1, pp. 19–24, Feb. 2007.

[51] J. C. Neu and W. Krassowska, "Asymptotic model of electroporation," *Phys. Rev. E*, vol. 59, no. 3, pp. 3471–3482, Mar. 1999.
[52] L. Rems *et al.*, "Cell electrofusion using nanosecond electric pulses," *Sci. Rep.*, vol. 3, 2013, Art. no. 3382.
[53] S. Mayer *et al.*, "Faradic resistance of the electrode/electrolyte interface," *Med. Biol. Eng. Comput.*, vol. 30, no. 5, pp. 538–542, Sep. 1992.
[54] R. A. Serway, *Principles of Physics*, 2nd ed. Fort Worth, TX, USA: Saunders, 1998.
[55] G. Serša *et al.*, "Vascular disrupting action of electroporation and electrochemotherapy with bleomycin in murine sarcoma," *Brit. J. Cancer*, vol. 98, no. 2, pp. 388–398, Jan. 2008.
[56] N. Dujardin *et al.*, "In vivo assessment of skin electroporation using square wave pulses," *J. Controlled Release.*, vol. 79, no. 1–3, pp. 219–227, Feb. 2002.
[57] S. A. Gallo *et al.*, Characterization of electric-pulse-induced permeabilization of porcine skin using surface electrodes," *Biophys. J.*, vol. 72, no. 6, pp. 2805–2811, Jun. 1997.
[58] U. Pliquett and C. Gusbeth, "Surface area involved in transdermal transport of charged species due to skin electroporation," *Bioelectrochemistry*, vol. 65, no. 1, pp. 27–32, Dec. 2004.
[59] U. Pliquett and M. R. Prausnitz, "Electrical impedance spectroscopy for rapid and noninvasive analysis of skin electroporation," *Methods Mol. Med.*, vol. 37, pp. 377–406, 2000.
[60] U. Pliquett, "Mechanistic studies of molecular transdermal transport due to skin electroporation," *Adv. Drug Del. Rev.*, vol. 35, no. 1, pp. 41–60, Jan. 1999.
[61] J. Zhuang and J. F. Kolb, "Time domain dielectric spectroscopy of nanosecond pulsed electric field induced changes in dielectric properties of pig whole blood," *Bioelectrochemistry*, vol. 103, pp. 28–33, Jun. 2015.
[62] M. Pavlin *et al.*, "Effect of cell electroporation on the conductivity of a cell suspension," *Biophys. J.*, vol. 88, no. 6, pp. 4378–4390, Jun. 2005.
[63] Y. Granot and B. Rubinsky, "Methods of optimization of electrical impedance tomography for imaging tissue electroporation," *Physiol. Meas.*, vol. 28, no. 10, pp. 1135–1147, Oct. 2007.
[64] M. Kranjc *et al.*, "Magnetic resonance electrical impedance tomography for measuring electrical conductivity during electroporation," *Physiol. Meas.*, vol. 35, no. 6, pp. 985–996, Jun. 2014.
[65] A. Ivorra *et al.*, "In vivo electrical conductivity measurements during and after tumor electroporation: Conductivity changes reflect the treatment outcome," *Phys. Med. Biol.*, vol. 54, no. 19, pp. 5949–5963, Oct. 2009.
[66] D. Cukjati *et al.*, "Real time electroporation control for accurate and safe in vivo non-viral gene therapy," *Bioelectrochemistry*, vol. 70, no. 2, pp. 501–507, May 2007.
[67] M. B. Sano *et al.*, "Towards the creation of decellularized organ constructs using irreversible electroporation and active mechanical perfusion," *Biomed. Eng. OnLine*, vol. 9, no. 1, p. 83, 2010.
[68] L. Davies *et al.*, "Modelling the effect of hydration on skin conductivity," *Skin Res. Technol.*, no. 23, pp. 363–368, 2016.
[69] K. C. Smith *et al.*, "Model of creation and evolution of stable electropores for DNA delivery," *Biophys. J.*, vol. 86, no. 5, pp. 2813–2826, May 2004.
[70] D. Šel *et al.*, "Finite-element modeling of needle electrodes in tissue from the perspective of frequent model computation," *IEEE Trans. Biomed. Eng.*, vol. 50, no. 11, pp. 1221–1232, Nov. 2003.
[71] D. E. Chafai *et al.*, "Assessment of the electrochemical effects of pulsed electric fields in a biological cell suspension," *Bioelectrochemistry*, vol. 106, pp. 249–257, Dec. 2015.
[72] R. Rodaite-Riseviciene *et al.*, "Release of iron ions from the stainless steel anode occurring during High-Voltage pulses and its consequences for cell electroporation technology," *IEEE Trans. Plasma Sci.*, vol. 42, no. 1, pp. 249–254, Jan. 2014.
[73] G. Saulis *et al.*, "Electrochemical processes during High-Voltage electric pulses and their importance in food processing technology," in *Advances in Food Biotechnology*, R. V. Rai, Ed. Chichester, U.K.: Wiley, 2015, pp. 575–592.
[74] G. Pataro *et al.*, "On the modelling of the electrochemical phenomena at the electrode-solution interface of a PEF treatment chamber: Effect of electrical parameters and chemical composition of model liquid food," *J. Food Eng.*, vol. 165, pp. 45–51, Nov. 2015.